

# DESIGN OF THE PRIMARY LIQUID-METAL PUMP OF THE MYRRHA RESEARCH REACTOR

*L. Mueller - T. Verstraete - T. Arts*

Turbomachinery and Propulsion Department, von Karman Institute for Fluid Dynamics  
Sint-Genesius-Rode, Belgium

lasse.mueller@vki.ac.be, tom.verstraete@vki.ac.be, tony.arts@vki.ac.be

## ABSTRACT

This paper presents the design of a liquid-metal pump for the primary cooling system of the advanced nuclear reactor MYRRHA conceived by the Belgian research center (SCK·CEN). The focus of this report is on the rotor design of the pump, as the most crucial component of the entire machine especially regarding erosion.

The single stage axial-flow pump has been designed with the optimization algorithm developed at the von Karman Institute for Fluid Dynamics (VKI) based on evolutionary methods. Two sequential optimization cycles have been applied to meet the required total head rise at design flow rate, while limiting the maximum velocity in the rotor tip section due to erosion.

In the preliminary design phase, the meridional flow path and rotational speed have been assessed by a 1D-model in the hub, mid, and tip section of the rotor. The outcome of this rather simple but very fast approach is a moderate specific speed, high hub-to-tip ratio rotor of  $N_s = 70$  and  $R_{hub}/R_{tip} = 0.88$ , respectively. In the second design step, accurate 3D-Navier-Stokes computations have been performed to design and automatically optimize the entire pump comprising the inlet section, the rotor and stator blade rows, and the diffuser. The high fidelity CFD analysis has been assisted by an Artificial Neural Network (ANN) to accelerate the optimization and to reduce the computational cost.

## NOMENCLATURE

### Latin

$c$	chord
$C_p$	pressure coefficient
$D$	diameter
$g$	acceleration due to gravity
$h$	enthalpy
$H$	head
$N$	number of blades
$N_s$	specific speed
$p$	pitch
$P$	pressure
$Q$	flow rate
$R$	radius
$Re_{inlet}$	inlet Reynolds number (Eqn.7)
$s$	meridional length
$U$	peripheral speed
$V$	absolute velocity
$W$	relative velocity
<u>Greek</u>	
$\alpha$	absolute flow angle

$\beta, \beta_m$	relative flow angle, blade metal angle
$\Delta$	delta/difference
$\eta$	efficiency
$\theta$	circumferential component
$\mu$	dynamic viscosity
$\nu$	hub-to-tip ratio
$\rho$	density
$\sigma$	solidity
$\omega$	angular rotational speed
$\phi$	flow coefficient (Eqn.16)
$\psi$	head coefficient (Eqn.14)
<u>Subscripts and Superscripts</u>	
$0, ref$	reference quantity
1	quantity upstream of the rotor
2	quantity downstream of the rotor
$hub, tip$	hub section, tip section
$hyd$	hydraulic
$tot$	total quantity
$x, m$	axial, meridional

ANN	Artificial Neural Network
DE	Differential Evolution
DOE	Design Of Experiments
MYRRHA	Multi-purpose, HYbrid Research Reactor for High-technology Applications
Obj	Objective
PS, SS	Pressure Side, Suction Side
RPM	Revolutions Per Minute

## INTRODUCTION

The MYRRHA project initiated by the Belgian nuclear research center (SCK·CEN) is aimed at constructing and operating a flexible fast spectrum experimental facility. It is conceived as an accelerator driven system (ADS), able to operate in sub-critical and critical modes (SCKCEN, 2012) and will allow the demonstration and performance assessment of the transmutation concept and associated technologies starting in 2023.

The primary system of the MYRRHA research reactor is a pool-type design, as illustrated in Fig. 1. All components of the primary loop, i.e. the pumps, heat exchangers, fuel handling tools, experimental rigs, etc., are inserted from the top and immersed in the reactor vessel, which is filled with lead-bismuth eutectic (LBE) as primary coolant. The relatively high boiling temperature of LBE of 1670°C leads to a passively safe design regarding a loss of coolant accident (LOCA), as it allows the operation without pressurizing the reactor even at high temperatures. However, the high density of LBE of 10,000 kg/m<sup>3</sup> adds additional restrictions to the primary pump. To avoid excessive erosion inside the pump, especially in the rotor tip section, the maximum relative velocity is limited to rather low values, e.g. pumps OKBM (2012) has developed for reactors using LBE operate at maximum velocities of  $W_{max} = 25 - 30$  m/s.

Reducing the maximum velocity to limit erosion is an essential objective within the design task of the pump. This will be accomplished using advanced evolutionary optimization methods.

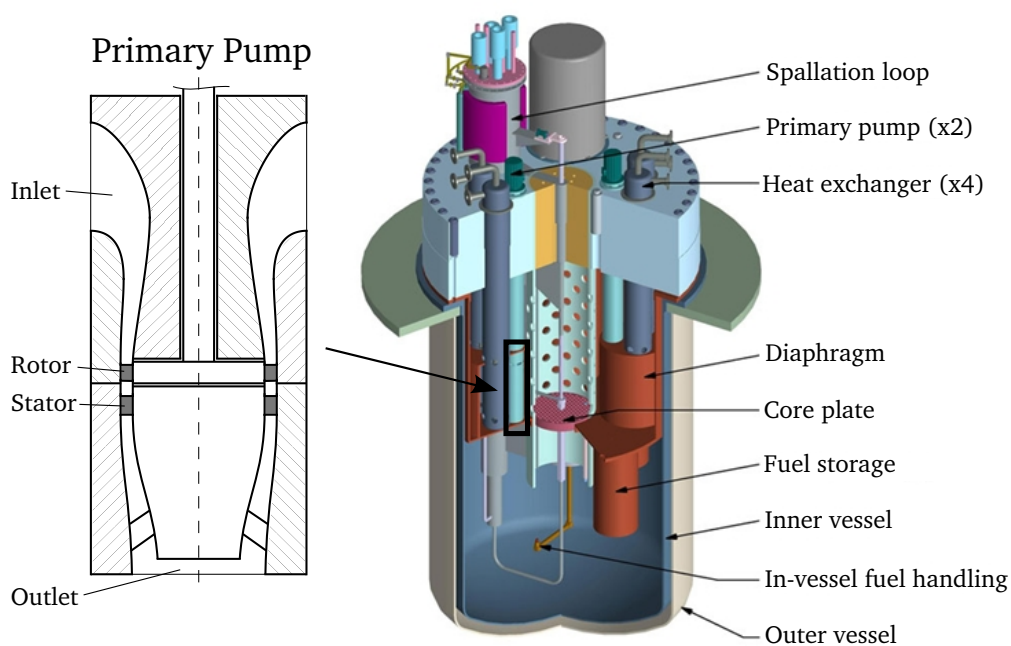


**Figure 1: Schematic Assembly of the MYRRHA Reactor (SCKCEN, 2012) With a Close Up on the Primary Pump (Dimensions Not to Scale)**

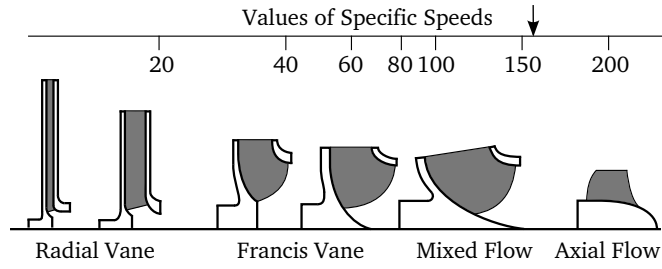


**Figure 2: Specific Speed Chart**

## DESIGN PROCEDURE

The choice of the machine type (axial flow, mixed flow, or radial flow) is related to the design requirements of the pump, i.e. to the flow rate  $Q$  and the total head  $\Delta H$ . A classical parameter in the selection of hydraulic machinery is the specific speed

$$N_s = \frac{RPM \sqrt{Q}}{\Delta H^{3/4}}. \quad (1)$$

Based on the design requirements of the MYRRHA pump provided by SCK·CEN the specific speed is in the range of mixed to axial-flow pumps  $N_s \approx 156$  (see Fig. 2). Although towards lower RPM a mixed-flow configuration might provide higher efficiency, an axial-flow pump is regarded as the best trade-off solution due its lower mechanical complexity and simplified manufacturing.

The use of preliminary design tools in the design process is recommended as it allows evaluating rapidly various design choices. Especially with regard to the erosion induced requirement of low relative velocity, it was decided to analyze various design options in this preliminary design phase. For that reason a simple one-dimensional model has been applied in the hub, mid, and tip section of the rotor to assess the meridional flow path and its rotational speed (Fig. 3, left). This rather simple model based on velocity triangles up- and downstream of the rotor blade allows a rapid screening of several design parameters, such as blade angles, rotational speed (RPM), and hub and tip radii,  $R_{hub}$  and  $R_{tip}$ , respectively. Although it does not include complex flow features, e.g. flow deviation or even flow separation, it provides a good estimation of the initial rotor design as an input for the following 3D-optimization.

Input parameters to the 3D-optimization are the hub and tip radii ( $R_{hub}$  and  $R_{tip}$ ) and the RPM of the rotor as illustrated in Fig. 3, (right). These parameters were unchanged in the subsequent high fidelity 3D-optimization, in which the three dimensional design of the pump comprising the inlet section, the rotor and stator rows, and the diffuser has been performed.

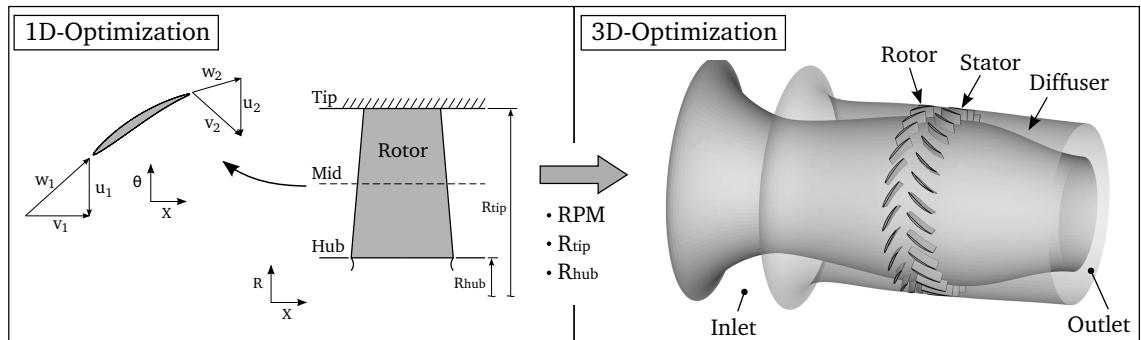


**Figure 3: Design Procedure**

## 1D OPTIMIZATION

### Computational Model

The 1D computational model is illustrated in Fig. 4. Input parameters are the hub and tip radii,  $R_{hub}$  and  $R_{tip}$ , and the RPM, next to the pump requirements ( $\Delta H$  and  $Q$ ). The axial velocity  $V_x$  is derived from the hub and tip radius for the specified flow rate  $Q$ . It is assumed at this stage that the axial velocity upstream of the rotor is constant from hub to tip although the pump will have a radial inlet bend (see Fig.1).

The peripheral speed  $U$  is computed at three sections (hub, mid and tip) from the rotational speed and the respective radii. The mid section is positioned in the middle of the hub and tip radius:  $R_{mid} = 0.5 \cdot (R_{hub} + R_{tip})$ .

The inlet absolute velocity  $V_1$  is assumed to be axial (no pre-rotation), which allows to compute the relative velocity  $W_1$  and the relative flow angle  $\beta_1$ .

The quantities downstream of the rotor (index 2) are computed based on the required total head  $\Delta H$  and assuming no losses ( $\eta_{hyd} = 1.0$ ) using the Euler-equation for pure axial inlet flow ( $V_{1\theta} = 0$ )

$$\frac{g \cdot \Delta H}{\eta_{hyd}} = U_2 V_{2\theta} - U_1 V_{1\theta} = U_2 V_{2\theta}. \quad (2)$$

and assuming the axial velocity  $V_x$  to maintain constant through the rotor (i.e. free vortex design). The absolute velocity downstream of the rotor  $V_2$ , the absolute flow angle  $\alpha_2$ , the relative velocity  $W_2$ , and the relative flow angle  $\beta_2$  are computed as illustrated in Fig. 4.

### Objectives and Constraints

Three design parameters (hub radius  $R_{hub}$ , tip radius  $R_{tip}$ , and RPM) can be chosen to obtain the required total head  $\Delta H$  and flow rate  $Q$ . However, additional requirements need to be imposed:

- The turning of the flow in the rotor ( $\beta_2 - \beta_1$ ) needs to be limited to reduce the losses, not accounted for in this preliminary design phase. According to Stepanoff (1957) the turning is limited to  $30^\circ$  to  $25^\circ$ .
- The diffusion in the rotor ( $W_2/W_1$ ) needs to remain feasible. A limit of 0.72 is often used, known as the de Haller number (Saravanamuttoo et al., 2001).
- The maximum relative velocity in the rotor  $W_{max}$  needs to remain at low values (10 - 20 m/s) to limit erosion.
- The absolute exit flow angle ( $\alpha_2$ ) needs to be small (from axial direction) to perform a feasible diffusion in the subsequent stator (Stepanoff, 1957).

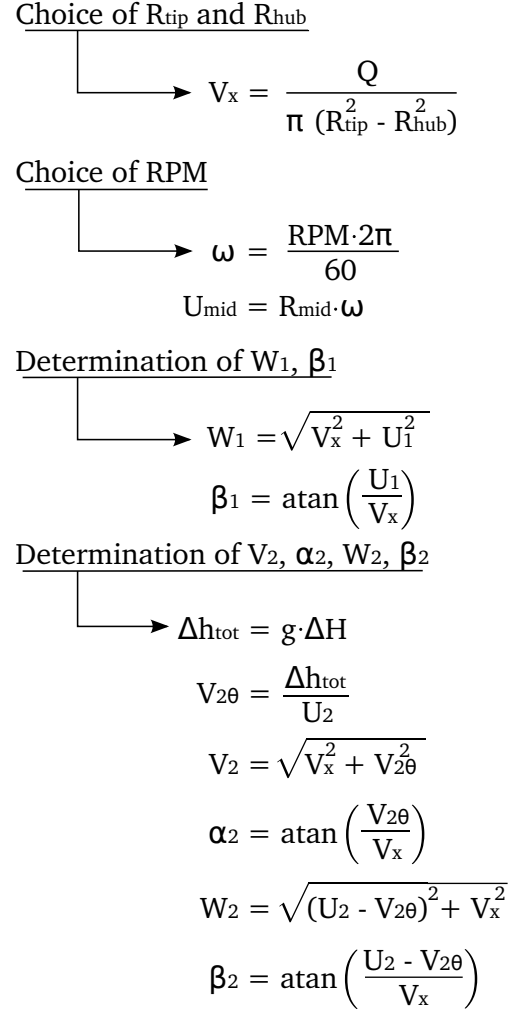


**Figure 4: 1D Computational Model**

The corresponding optimization problem is formulated as:

$$\text{Minimize: } Obj_1 = W_1^{tip} \quad (3)$$

$$Obj_2 = -W_2^{hub}/W_1^{hub} \quad (4)$$

$$\text{Subject to: } Constr_1 = abs(\beta_2^{hub} - \beta_1^{hub}) \leq \Delta\beta_{max} \quad (5)$$

$$Constr_2 = V_x \leq V_{x,max} \quad (6)$$

The first objective  $Obj_1$  (Eqn. 3) reduces the maximum relative velocity in the rotor, which is in the tip section at the inlet. A value in the range of  $W_1^{tip} = 10$  to  $20$  m/s is considered as feasible, although lower values are preferred, as they would increase the lifetime with respect to erosion. The second objective  $Obj_2$  (Eqn. 4) maximizes the diffusion ratio near the hub to prevent an excessive diffusion. For a free vortex design the highest diffusion occurs in the hub section. The first constraint Eqn. 5 restricts the turning at the hub, where the largest relative flow turning will take place, while the second constraint (Eqn. 6) puts an additional limitation on the axial velocity to limit the erosion risk in the meridional passage.

### Methodology

Three different design variables are allowed to be changed during the preliminary design phase, i.e. the hub and tip radii ( $R_{hub}$  and  $R_{tip}$ ) and the rotational speed RPM. Each design variable is allowed to change within a specified range. For each choice of the hub radius  $R_{hub}$ , tip radius  $R_{tip}$ , and RPM, the velocity triangles can be computed by the 1D model and the requirements can be evaluated. In order to find the three design parameters that give a suitable compromise for the diffusion  $W_2/W_1$ , turning  $\Delta\beta$ , and maximum velocity  $W_{max}$  requirements, a Differential Evolutionary (DE) algorithm (Storn and Price, 1997) has been used. Figure 5 illustrates schematically the optimization flowchart.

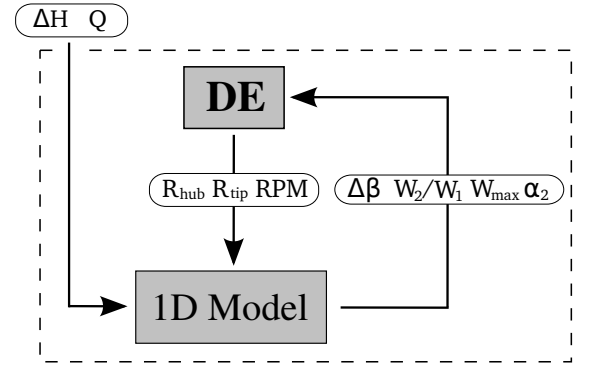
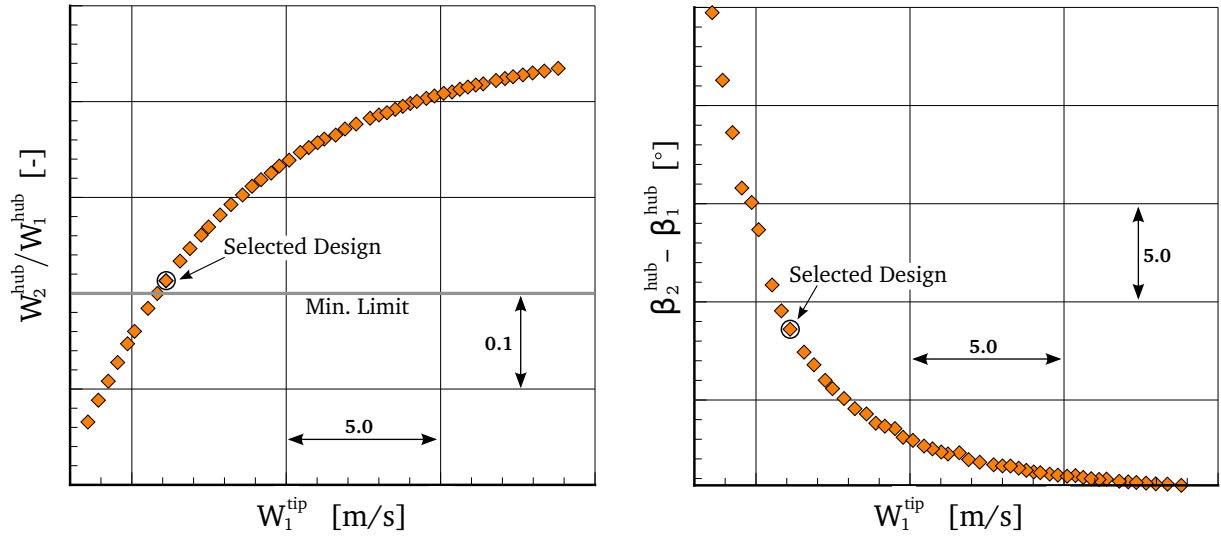


Figure 5: 1D Optimization Flowchart

### Results

The results of the 1D optimization are illustrated in Fig. 6, showing both the diffusion in the hub section  $W_2^{hub}/W_1^{hub}$  (left) and the flow turning  $\beta_2^{hub} - \beta_1^{hub}$  (right) with respect to the relative velocity in the rotor tip section  $W_1^{tip}$ . A Pareto front is found instead of one single optimal design, which is typical of multi-objective optimization. This is a set of so called non-dominated designs, in which one objective cannot be improved without worsening the other. In Fig. 6, (left), a clear Pareto front (towards the upper left hand corner) is visible indicating that a lower maximum velocity  $W_1^{tip}$  comes at the expense of a larger diffusion near the hub (lower  $W_2^{hub}/W_1^{hub}$ ). This evidently results also in a higher flow turning near the hub, as can be seen in Fig. 6, (right). The resulting Pareto front allows the designer to select designs depending on the weight given to each objective. In the present case, it was decided to select the design with a hub diffusion ratio ( $W_2^{hub}/W_1^{hub}$ ) close to the minimum limit as indicated in Fig. 6, (left). This design has a specific speed of  $N_s \approx 70$  with a high hub-to-tip ratio of  $\nu = R_{hub}/R_{tip} = 0.88$ , which is larger than commonly used for axial (propeller-like) pumps in the range of  $\nu = 0.3 - 0.7$  (Stepanoff, 1957).



**Figure 6: Diffusion in the Hub vs. Relative Velocity in the Tip Section (left), Turning in the Hub Section vs. Relative Velocity in the Tip Section (right)**

However, this is due to the very low velocity requirement (i.e. low  $V_x$  and  $W_1^{tip}$ ) and high diffusion (i.e. low  $W_2^{hub}/W_1^{hub}$ ) for a single stage pump. Similar conclusions were drawn within a design study of axial pump rotors for liquid rocket application (Crouse and Sondercock, 1964; Miller and Crouse, 1965; Urasek, 1971). Several rotors (see Fig. 7) were designed and tested with hub-to-tip ratios between  $\nu = 0.4 - 0.9$  for a specified diffusion, which confirms the results obtained from this preliminary design optimization.

### 3D OPTIMIZATION

#### Methodology

The 3D design of the primary pump is performed with the optimization algorithm developed at the von Karman Institute (VKI) with special focus on turbomachinery applications. The system (Fig. 8) makes use of a Differential Evolution algorithm (DE), a metamodel based on an Artificial Neural Network (ANN), a database, and high fidelity simulation tools for the flow analysis (CFD).

The basic approach of this method is that the Artificial Neural Network substitutes the computational expensive tools for the CFD in the *Generation Loop* (see Fig. 8) and provides less accurate but very fast performance predictions to evaluate the large number of geometries necessary by the DE during its search for the optimum. However, the metamodel requires a validation which is then performed in the *Iteration Loop* according to Fig. 8. After a specified number of generations, the optimum geometries according to the ANN predictions are analyzed by the more accurate but much more computationally expensive CFD calculations to verify the accuracy of the metamodel. The results of the accurate performance analysis are added to the database and a new *Generation Loop* is started after a new training of the metamodel on the enlarged database. In this way the whole system is self-learning, resulting in a more accurate ANN.

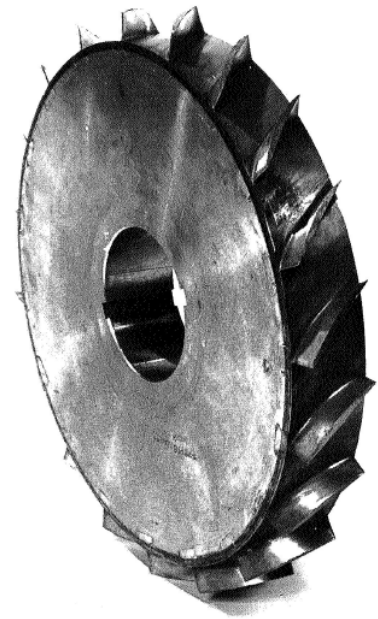


**Figure 7: NASA Axial Pump Rotor for Liquid Rocket Application (hub-to-tip ratio  $\nu = 0.9$ ) (Urasek, 1971)**

The Differential Evolution algorithm used was developed by Storn and Price (1997). In present optimization, 1000 generations are created with a constant population size of 40 individuals. To validate the ANN predictions in each *Iteration Loop* eight individuals were selected and reassessed by the high fidelity tools.

The initial sampling of the database was performed by means of a Design of Experiments (DOE) (Montgomery, 2006). The DOE is based on statistical methods and considers, that  $k$  design variables can take two values fixed at a specified position in the design space (here: 20% and 80% plus one central case = 50%). Further, to reduce the number of required evaluations, the fractional factorial design approach (Montgomery, 2006) is used:  $2^{(k-p)}$  with  $(k-p) = 6$ , thus resulting in 64 experiments plus the central case, which are the initial sampling of the database.

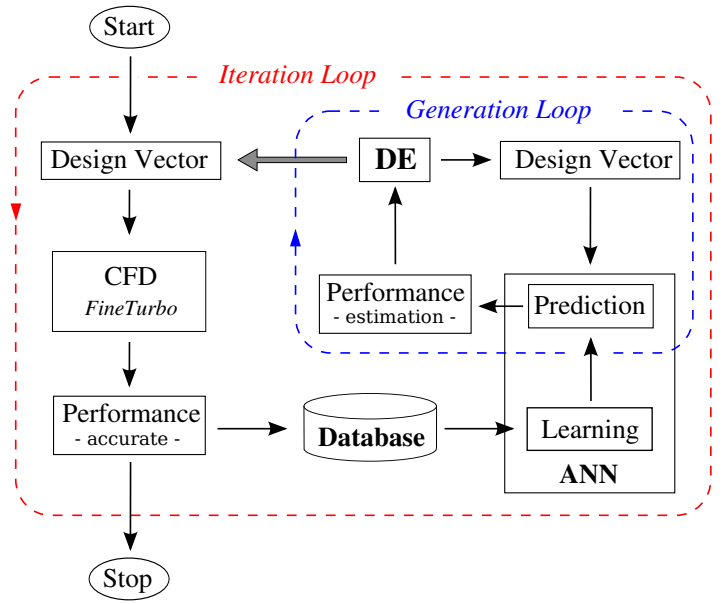


**Figure 8: VKI Optimization Algorithm**

### Parameterization

The 3D model of the rotor of the pump (cf. Fig. 1) is based on Bézier and B-spline curves and surfaces and is defined by:

1. the meridional contour,
2. the blade camber line at hub and tip,
3. the thickness distribution, which is added normal to the camber line at hub and tip, and
4. the number of blades.

The definition of the meridional contour is shown in Fig. 9. The meridional flow path is subdivided into different patches: an inlet patch (90°-bend and swan neck), a blade patch, and an outlet patch. The blade patch corresponds to where the rotor blade is located in the meridional plane. The coordinates of the control points are the geometrical parameters which can be modified by the optimization program and the possible variation in axial and radial direction is indicated by arrows. In order to have a good control about the geometry and to avoid undesirable shapes, lengths and angles are used (e.g.  $L_{10}$  to  $L_{10}$ ,  $H_{inlet}$ ,  $\alpha_{hub}$  and  $\alpha_{shroud}$ ). In total 15 parameters define the meridional flow path.

The rotor blade is defined by the blade camber line of the hub and tip section, each separately defined by the blade angle  $\beta_m$ -distribution with respect to the meridional plane. The  $\beta_m$ -distribution is parameterized by a Bézier curve with three control points, one at the leading and trailing edge and one intermediate control point. This results in a total of 6 degrees of freedom.

The final blade with the pressure and suction side surfaces is created by adding a thickness distribution normal to the camber line at hub and tip. In the present optimization study, a NACA 65 thickness distribution at hub and tip has been chosen, which shape is kept constant during the optimization process.

The number of blades, which defines the full rotor, is introduced as an optimization parameter within this design study. This parameter has a major effect on solidity, i.e. on the blade loading and on the blockage of the flow in case of accidents with no pump rotation, in which cooling needs to be guaranteed by natural convection in the reactor.

In total 22 parameters define the geometry of the pump and will be subject to optimization.

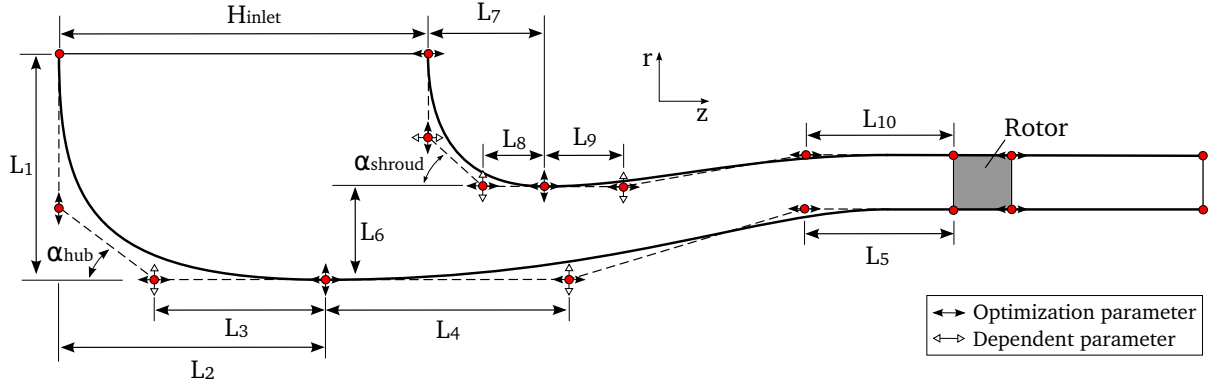


**Figure 9: Meridional Parameterization of the Inlet Section and the Rotor**

### Flow Analysis

Every geometry in the *Iteration Loop* according to Fig. 8 has been analyzed at the design operating point using the commercial flow solver fineTurbo<sup>TM</sup>. The incompressible Reynolds-Averaged Navier-Stokes (RANS) equations are solved using a Runge-Kutta scheme in conjunction with accelerating techniques such as variable-coefficient implicit residual smoothing and a multi-grid scheme. Discretization is based on finite volumes with a cell-centered scheme stabilized by artificial dissipation. For the turbulence closure the one equation model of Spalart and Allmaras (Wilcox, 1993) is used with the assumption of fully turbulent flow with an inlet Reynolds number of

$$Re_{inlet} = \frac{V_{inlet} R_{inlet} \rho}{\mu} = 6.5 \cdot 10^5 \quad (7)$$

where  $V_{inlet}$  and  $R_{inlet}$  are the absolute inlet velocity and the inlet radius, respectively. The flow properties of lead-bismuth eutectic (LBE) according to NEA (2008) have been used for the CFD simulations.

### Objectives and Constraints

The optimization of the inlet section and the rotor has two objectives:

1. Maximizing the hydraulic efficiency

$$Obj_1 = \eta_{hyd} = \frac{\Delta P_{tot}}{\rho \cdot \Delta(V_{\theta}U)} \quad (8)$$

where  $\rho$  is the density of LBE,  $\Delta P_{tot}$  the mass-flow averaged absolute total pressure rise, and  $\Delta(V_{\theta}U)$  the difference of the mass flow averaged angular momentum between inlet and outlet.

2. Reducing the maximum isentropic velocity  $(W/W_0)_{max,SS}$  on the blade suction side at 90% span. The isentropic velocity objective aims at reducing the maximum relative velocity in the tip section (90%-span) as shown in Fig. 10 and is computed as follows:

$$Obj_2 = (W/W_0)_{max,SS} = \sqrt{1 - C_p|_{min,SS}} \quad (9)$$

with the pressure coefficient  $C_p$ :

$$C_P = \frac{P - P_{ref}}{0.5 \cdot \rho \cdot W_{ref}^2} \quad (10)$$

The two objectives are subject to two constraints:

$$Constr_1 = \Delta H \geq \Delta H_{min} \quad (11)$$

and

$$Constr_2 = [(W/W_0)_{max,ps} - (W/W_0)_{max,ss}] \leq 0. \quad (12)$$

The first constraint (Eqn. 11) ensures that the designs generated by the optimization program supply the required total head for the design flow rate. The second constraint (Eqn. 12) prevents that the isentropic velocity objective  $Obj_2$  is not improved at the expense of a higher velocity on the pressure side at the leading edge due to negative incidence, i.e. if the flow impinges on the suction side, which results in a velocity peak on the pressure side (Fig. 10).

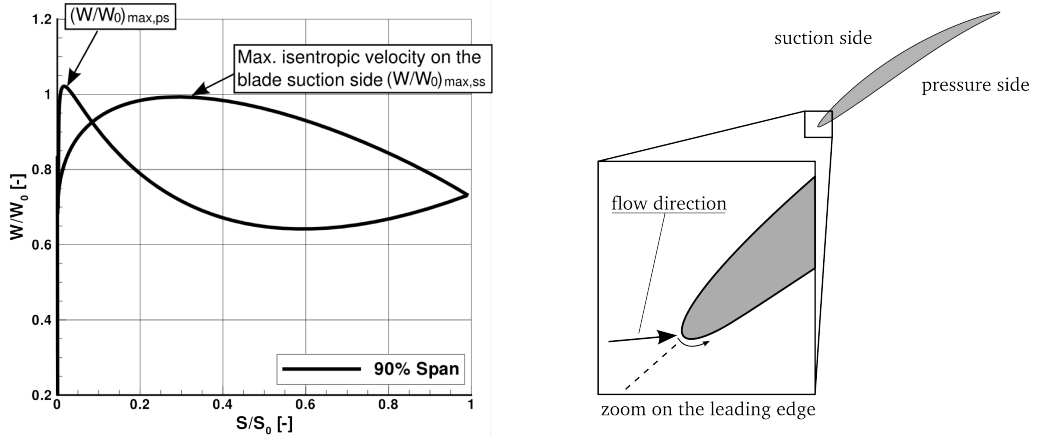


**Figure 10: Illustration of negative incidence resulting in a velocity peak on the pressure side**

## Results

The results of the optimization are presented in Fig. 11, showing both the total head  $\Delta H$  (left) and the maximum isentropic velocity on the suction side  $(W/W_0)_{max,SS}$  (right) with respect to the hydraulic efficiency  $\eta_{hyd}$ . Each symbol in Fig. 11 represents one design that has been analyzed by CFD. The square symbols represent the geometries analyzed for the initial database (DOE) prior to the optimization to train the metamodel. The designs generated during the optimization process are the diamond shape symbols. From the initial scattered distribution of the DOE (Fig. 11, left), the optimizer generated a large number of designs with high hydraulic efficiency  $\eta_{hyd}$  and minimum required total head (indicated with the horizontal line in Fig. 11). The selected design of this optimization supplies a total Head, which is above the minimum required value, with high hydraulic efficiency. The reason why this particular design has been chosen is more obvious from Fig. 11, (right) showing the two-dimensional objective space, i.e. the maximum isentropic velocity on the suction side  $(W/W_0)_{max,SS}$  with respect to the hydraulic efficiency  $\eta_{hyd}$ .

In this plot only designs which satisfy the constraints according to Eqns. 11 and 12 are presented such that the apparent front of designs towards the lower right hand corner is the Pareto front comprising non dominated designs, i.e. no other designs outperform the Pareto optimal designs with respect to both higher efficiency and lower relative velocity. Higher hydraulic efficiency comes at the expense of higher relative velocity due to positive incidence resulting in a velocity peak on the suction side leading edge. In this optimization reducing the isentropic velocity on the suction side, i.e. the relative velocity to limit erosion had a higher priority than improving the efficiency, resulting in the selected design, which is considered as the best trade-off solution of both objectives.

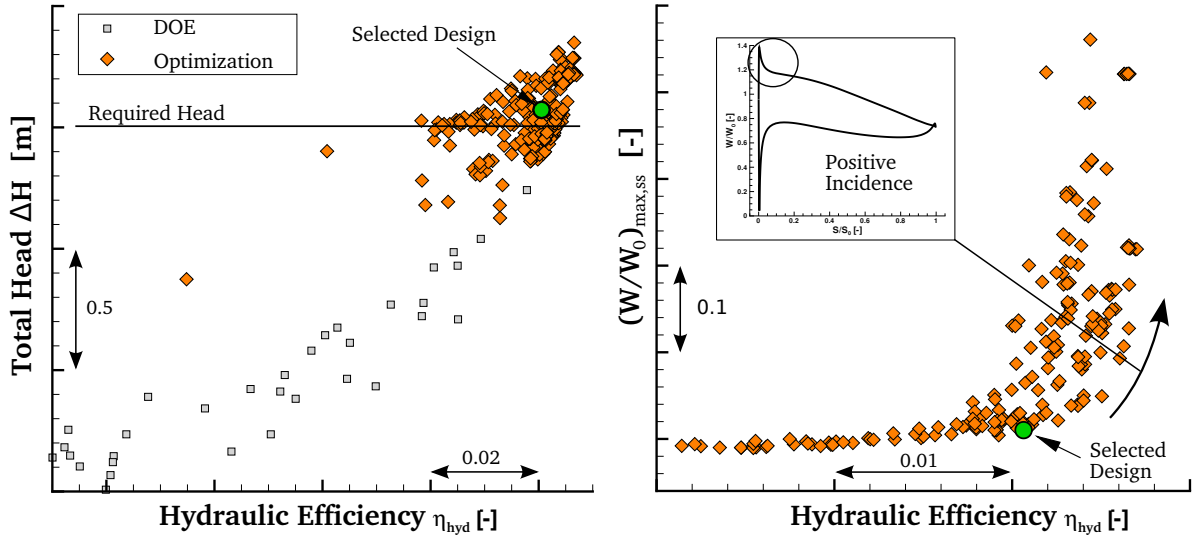


**Figure 11: Total Head vs. Hydraulic Efficiency (left), 2D Objective Space:  $(W/W_0)_{max,SS}$  vs. Hydraulic Efficiency (right)**

The selected design, which is presented in Fig. 12, (left) is a high staggered, low aspect ratio rotor ( $h/c_{tip} \approx 0.36$ ) with a solidity in the tip section of  $(c/p)_{tip} \approx 1.26$ . It is a mid-loaded blade with an equal loading in the hub and tip section and with a smooth diffusion on the suction side as illustrated in Fig. 12, (middle) showing the isentropic velocity distribution at 10% and 90% span. Additionally, as illustrated already in the 2-dimensional objective space in Fig. 11, (right), this design has a rather low velocity on the suction side which limits the erosion risk. Figure 12, (right) illustrates the mass-flow averaged span-wise distribution of the rotor Diffusion Factor (DF) at design operating conditions. Although the Diffusion Factor introduced by Lieblein et al. (1953)

$$DF = 1 - \frac{W_2}{W_1} + \frac{\Delta W_\theta}{2\sigma W_1} \quad (13)$$

using the relative velocities up- and downstream of the rotor and the solidity  $\sigma$  is strictly valid for two-dimensional flows, it is a suitable parameter to estimate off-design tendencies. Except close to the side walls where the flow is overturned due to secondary flows (i.e. due to the hub and shroud passage vertices), the computed rotor Diffusion Factor is below  $DF \leq 0.5$ , which indicates a sufficient margin towards lower flow rates.

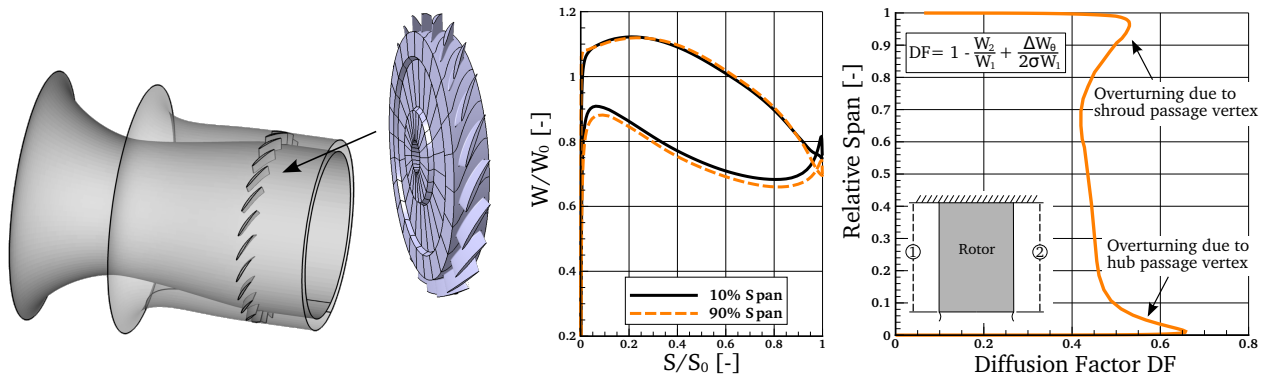


**Figure 12: Selected Design Indicated in Fig. 11 with a Close Up on the Rotor (left), Isentropic Velocity Distribution at 10% and 90% Span (middle), Span-wise Distribution of Rotor Diffusion Factor (right)**

### Stator-Diffuser Optimization

Subsequently to the inlet-rotor design optimization, the stator-diffuser has been designed and optimized. A similar parameterization as for the inlet-rotor optimization is used with 18 degrees of freedom, comprising the meridional flow path and blade shape. The design of the rotor is kept constant during this process, but the inlet and rotor are modeled in the CFD during this design effort. The objectives of the optimization are to diffuse as much as possible inside the diffuser with limited losses, while reducing as much as possible the velocity peak on the suction side of the stator vane to limit erosion. The outcome of this optimization is illustrated in Fig. 13, showing the meridional velocity with a span-wise distribution upstream of the rotor and the isentropic velocity distribution at 10% and 90% span of the stator vane.

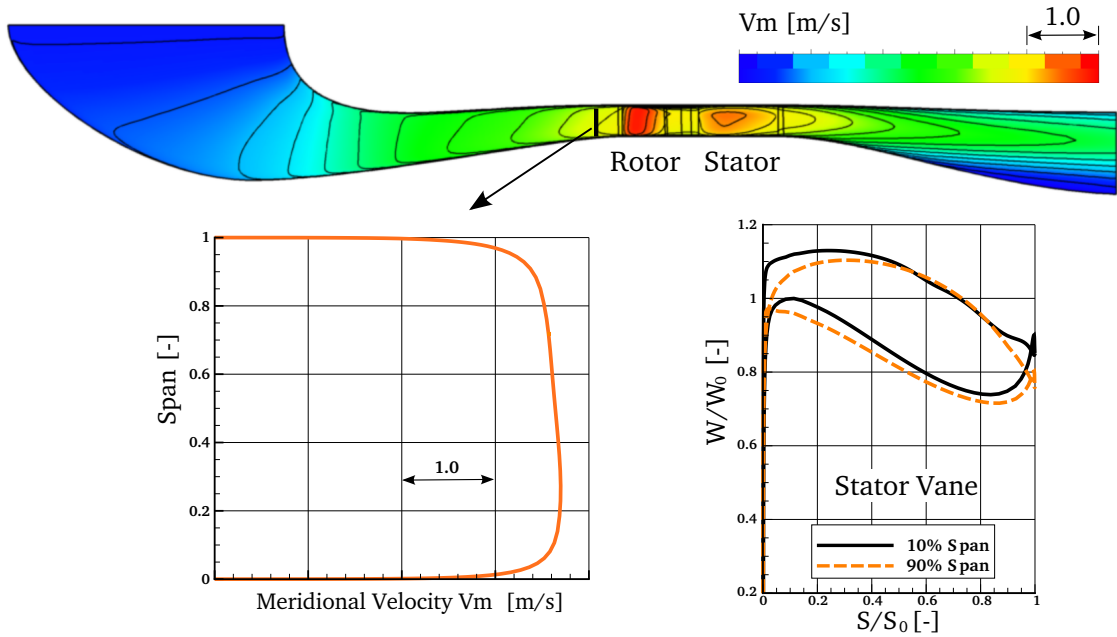


**Figure 13: Meridional Velocity in the Final Pump Design and Isentropic Velocity Distribution at 10% and 90% Span of the Stator Vane**

### Performance Map

The selected design (Fig. 13) has been analyzed further regarding its off-design performance. Although the pump was designed primarily for the design point, it has good off-design characteristics, which is illustrated in Fig. 14, showing the Head coefficient

$$\psi = \frac{g \cdot \Delta H}{U_{tip}^2} \quad (14)$$

and the efficiency based on the torque

$$\eta_{Torque} = \frac{\dot{m} \Delta H g}{\omega \cdot Torque} \quad (15)$$

with respect to the flow coefficient

$$\phi = \frac{V_x}{U_{tip}} \quad (16)$$

The reason for the good off-design behavior is related to the chosen design strategy. The optimization was aiming at limiting the diffusion in the rotor and stator and reducing the incidence of both blade rows resulting in a robust design with an entirely sufficient negative slope ( $\equiv \Delta\psi/\Delta\phi$ ) of the characteristics curve.

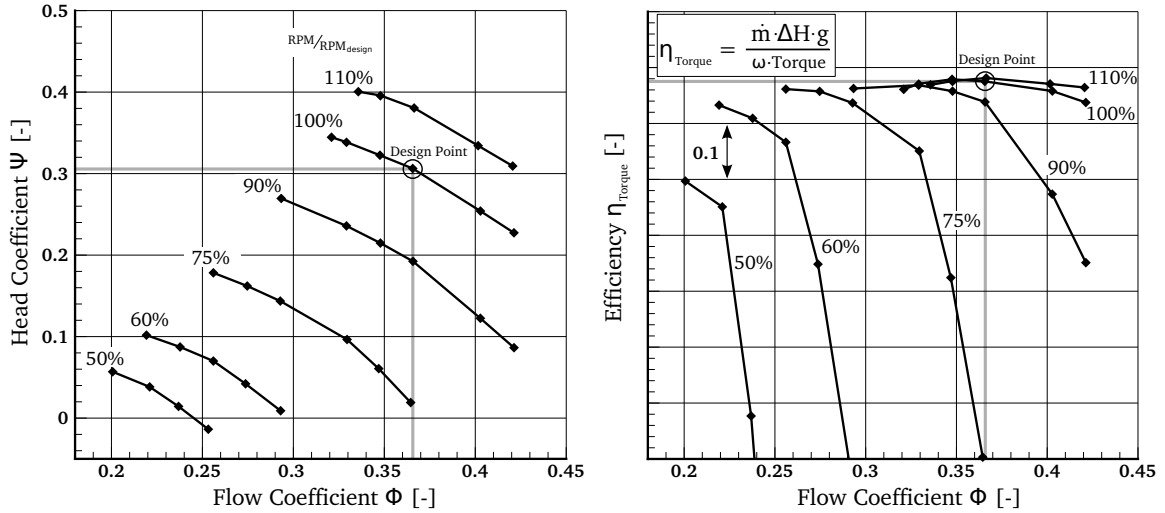


**Figure 14: Performance Map of the Pump**

## CONCLUSIONS

A hydrodynamic optimization based on evolutionary methods is used to design the primary pump of the MYRRHA nuclear reactor. The design approach is aimed at

- maximizing the hydraulic efficiency of the rotor,
- minimizing the pressure losses in the stator and diffuser, and
- reducing the relative velocity in the rotor tip section

Based on the preliminary 1D optimization, the rotor and stator have been designed in two successive steps keeping the number of design parameters and objectives to feasible values in each optimization run. The outcome is a pump, which supplies the required Head and is respecting the design target of low relative velocity to limit erosion.

The pump has been realized as a moderate specific speed, high hub-to-tip ratio axial pump ( $N_s = 70$ ,  $R_{hub}/R_{tip} = 0.88$ ), although a mixed-flow pump would provide higher hydraulic efficiency according to classical specific speed charts. However, due to the additional complexity of a mixed flow configuration in the manufacturing process, an axial configuration is more attractive.

Although the pump was designed primarily for the design operating point, it has a good off-design behavior, which is the result of the chosen design strategy. The optimization was aiming at limiting the diffusion in the rotor and stator and reducing the incidence of both blade rows resulting in a robust design.

## ACKNOWLEDGEMENTS

The financial support of the Belgian Science Policy Office (BELSPO) is gratefully acknowledged.

## References

- Crouse, J. and Sondercock, D. (1964). Blade-Element Performance of 0.7 Hub-Tip Radius Ratio Axial-Flow Pump rotor with Tip Diffusion Factor of 0.43. Technical Report NASA TN D-2481, Lewis Research Center, Cleveland Ohio.
- Lieblein, S., Schwenk, F. C., and Broderick, R. (1953). Diffusion Factor for Estimating Losses and Limiting Blade Loadings in Axial-Flow-Compressor Blade Elements. Technical Report NACA RM E53D01, Lewis Flight Propulsion Laboratory, Cleveland Ohio.
- Miller, M. and Crouse, J. (1965). Design and Overall Performance of an Axial-Flow Pump Rotor with a Blade-Tip Diffusion of 0.66. Technical Report NASA TN D-3024, Lewis Research Center, Cleveland Ohio.
- Montgomery, D. (2006). *Design and Analysis of Experiments*. John Wiley & Sons, Inc.
- NEA (2008). Handbook on Lead-bismuth Eutectic Alloy and Lead Properties, Materials Compatibility, Thermal-hydraulics and Technologies. <http://www.oecd-nea.org/science/reports/2007/nea6195-handbook.html>.
- OKBM (2012). Experimental Designing Bureau of Machine Building. <http://www.okbm.nnov.ru/>.
- Saravanamuttoo, H., Rogers, G., Cohen, H., and P.V., S. (2001). *Gas Turbine Theory*. Pearson Prentice Hall., 5 edition.
- SCKCEN (2012). Myrrha: Multi-purpose hybrid research reactor for high-tech applications. <http://myrrha.sckcen.be/>.
- Stepanoff, A. (1957). *Centrifugal and Axial Flow Pumps*. John Wiley & Sons, Inc.
- Storn, R. and Price, K. (1997). Differential Evolution - A Simple and Efficient Heuristic for Global Optimization over Continuous Spaces. *Journal of Global Optimization*, 11:341–359.
- Ursek, D. (1971). Design and Performance of a 0.9 Hub-Tip-Ratio Axial-Flow Pump Rotor with a Blade-Tip Diffusion Factor of 0.63. Technical Report NASA TM X-2235, Lewis Research Center, Cleveland Ohio.
- Wilcox, D. (1993). *Turbulence Modelling for CFD*. DCW. Industries, Inc.